

1 **Evolution of sea-surface conditions on the northwestern Greenland margin**
2 **during the Holocene**

3 MYRIAM CARON^{1,*}, ANDRE ROCHON¹, JEAN-CARLOS MONTERO-SERRANO¹, GUILLAUME
4 ST-ONGE^{1,2}

5 ¹ Institut des sciences de la mer de Rimouski (ISMER), Université du Québec à Rimouski and GEOTOP Research
6 Center, Canada ; ² Canada Research Chair in Marine Geology

7
8 *Acknowledgments.* We are grateful to the captain, officers, crew and scientists on board the CCGS
9 Amundsen during the 2014 ArcticNet (Leg 1b) expedition for the recovery of cores 204 and
10 Kane2B. This study was supported by ArcticNet, the Natural Sciences and Engineering Research
11 Council of Canada (NSERC) through Discovery Grants to AR, JCMS and GSO, and the CREATE
12 ArcTrain program through a PhD scholarship to the first author. We thank J. Matthiessen (Alfred-
13 Wegener Institute) for useful advice on dinocyst identification and Q. Beauvais and M-P. St-Onge
14 (UQAR-ISMER) for technical support in the laboratory. We also thank G. Massé (Takuvik) for
15 collecting the cores, MM. Ouellet-Bernier (UQAM) for sharing the MSM343300 sea-surface
16 reconstructions data, as well as E. Georgiadis and J. Giraudeau (U. Bordeaux) for fruitful
17 discussions. Finally, we thank the two anonymous reviewers for their thorough and critical
18 comments, which helped to improve the manuscript.

19
20 **ABSTRACT**

21 Reconstructions of sea-surface conditions during the Holocene were achieved on two sediment
22 cores from the Northwest Greenland margin (AMD14-204) and Kane Basin (AMD14-Kane2B)
23 based on dinoflagellate cyst assemblages. On the northwest Greenland margin, sea-surface
24 conditions were cold with an extended sea-ice cover prior to 7750 cal a BP associated to the end
25 of the deglaciation. A major change occurred around ca. 7750 cal a BP with enhanced influence of
26 warmer water from the West Greenland Current (WGC), and optimal sea surface conditions were
27 observed around 6000 cal a BP. After 3350 cal a BP, results reflect establishment of the modern
28 assemblages. In the Kane Basin, sea-surface conditions were not favorable for dinocysts
29 productivity prior 7880 cal a BP, as the basin was still highly covered by ice. Presence of warmer
30 water is recorded between 7880 and 7200 cal a BP and highest primary productivity between 5200
31 and 2100 cal a BP, but sea-surface conditions remained cold with an extended sea-ice cover
32 throughout the Holocene. Overall, the results from this study revealed the strong influence of
33 meltwater discharges and oceanic current variability on the sea-surface conditions.

34 **KEYWORDS.** Dinoflagellate cysts; Baffin Bay; Melville Bay; Kane Basin; Sea surface conditions

35 * Corresponding author: M. Caron, UQAR-ISMER and GEOTOP.
36 E-mail: myriam.caron03@uqar.ca

1 **Introduction**

2 Over the last decades, the Arctic has strongly responded to modern climate warming with the
3 reduction of sea-ice extent and cover duration (Serreze and Stroeve, 2015) and to place these rapid
4 changes in a long-term perspective, there is a need for a better understanding of the interactions
5 between sea ice and climate throughout the geological past (Jakobsson *et al.*, 2010; Müller and
6 Stein, 2014). Baffin Bay is an excellent location to study these interactions as sea-ice is present
7 inside the bay during most of the year (Tang *et al.*, 2004) and because it plays the role of oceanic
8 corridor between the Arctic and the North Atlantic oceans (through Labrador Sea, where deep
9 convection contributes to the thermohaline circulation). Moreover, Baffin Bay has been affected
10 by the dynamics of three large ice sheets (Greenland [GIS], Innuitian [IIS] and Laurentide [LIS]
11 ice sheets) since the last glacial maximum (England *et al.*, 2006). Therefore, it is highly relevant to
12 investigate how oceanographic and climatic changes affected the sea surface conditions in Baffin
13 Bay since the last deglaciation.

14 Dinoflagellates cysts (hereafter, dinocysts) are excellent tracers for the estimation of past sea-
15 surface conditions, as their highly resistant organic membrane (e.g., Fensome *et al.*, 1993) allows
16 them to be preserved in the sediment, particularly in subpolar and polar seas where they are found
17 in abundance and high diversity (e.g., Mudie, 1992; Matthiessen, 1995; Mudie *et al.*, 2001). Several
18 oceanographic properties can be reconstructed from dinocyst assemblages including sea-surface
19 temperature (SST), salinity (SSS), seasonal sea-ice cover (SIC), and primary productivity (de
20 Vernal *et al.*, 2001, 2013a; Radi and de Vernal, 2008). Previous studies based on dinocysts, but
21 also diatoms, mollusk, foraminifera and sea ice biomarkers (IP₂₅) have contributed to improving
22 our knowledge of past sea-surface conditions in Baffin Bay (e.g., Knudsen *et al.*, 2008; Krawczyk
23 *et al.*, 2017). However, information available on the northeastern Baffin Bay (Melville Bay) and

1 Nares Strait sea-surface variability during the Holocene is still incomplete, as studies have mainly
2 been focused on the regions of the North Water Polynya (e.g., Levac *et al.*, 2001) and Disko Bay
3 region (e.g., Ribeiro *et al.*, 2012; Allan *et al.*, 2018). In this study, well-preserved dinocyst
4 assemblages of two sediment cores recovered from the Upernavik cross-shelf trough (AMD14-
5 204) and in the Kane Basin (AMD14-Kane2B) were analyzed and data was processed with the
6 modern analogue technique (MAT) to reconstruct sea-surface conditions during the Holocene.

7 **Environmental setting**

8 Baffin Bay is an oceanic basin 1300 km long and 450 km wide, with a depth of up to 2300 m (Aksu
9 and Piper, 1987). It is connected to the Arctic Ocean through CAA straits and to the Atlantic Ocean
10 through Davis Strait. Nares Strait separates Ellesmere Island from Greenland and extends North of
11 Baffin Bay up to the Arctic Ocean (Fig. 1). Baffin Bay is influenced by the cold Baffin Island
12 Current (BIC, temperature $>-1^{\circ}\text{C}$, salinity <34) flowing southward along Baffin Island from
13 northernmost Baffin Bay, and by the relatively warm and salty West Greenland Current (WGC;
14 temperature $>2^{\circ}\text{C}$, salinity >34) flowing northward (Fig. 1; Tang *et al.*, 2004 ; Zweng and
15 Münchow, 2006). The WGC consists of a mix of the cold and low salinity East Greenland Current
16 (EGC; arctic water from Fram Strait) and the warmer and salty Irminger Current (IC; North Atlantic
17 water), both of which merge south of Greenland to form the WGC (Fig.1; Tang *et al.*, 2004). The
18 WGC flows northward along the west Greenland shelf and turns west in Melville Bay before
19 joining the BIC in Smith Sound. However, it has been shown that a small branch of the WGC
20 reaches Kane Basin and circulates at depths below 250 m (Sadler, 1976). Baffin Bay is covered by
21 sea-ice during most of the year, with a minimal extent in September (Tang *et al.*, 2004).
22 Nevertheless, the SIC distribution in Baffin Bay is asynchronous with sea-ice extending further
23 southward on the east than the west side due to the differences in temperature and salinity of the

1 two major surface currents (WGC and BIC) flowing in opposite directions (Tang *et al.*, 2004). Ice
2 floes and icebergs are present continually in Nares Strait, even during summer (Münchow *et al.*,
3 2006). Landfast ice during winter leads to the formation of an ice arch in Kane Basin, which marks
4 the boundary with the North Water Polynya (Barber *et al.*, 2001; Kwok *et al.*, 2010).

5 **Material and methods**

6 Two Calypso Square (CASQ) cores were collected on board the CCGS icebreaker Amundsen in
7 northern Baffin Bay during the 2014 ArcticNet expedition: core AMD14-204 (hereinafter referred
8 to as 204) located on the northwest Greenland margin, and core AMD14-Kane2B (hereinafter
9 referred to as Kane2B) located in the Kane Basin (Fig. 1; Table 1). The chronology of core 204
10 was established using an approach combining radiocarbon dating ($\Delta R = 140 \pm 30$ years) with
11 paleomagnetic chronostratigraphic markers (Caron *et al.*, 2019) and organic matter dating
12 (Giraudeau *et al.*, under review). The chronology of core Kane2B was established by Georgiadis
13 *et al.* (2018) based on twenty radiocarbon ages from mixed benthic foraminifera and mollusk shell
14 fragments ($\Delta R = 240 \pm 51$ years). Based on the established chronologies, core 204 covers the last
15 ca. 9100 cal a BP, and has a mean sedimentation rate of 95 cm ka^{-1} , while core Kane2B covers the
16 last ca. 9000 cal a BP, and has sedimentation rates ranging from 20 to 220 cm ka^{-1} (Fig. S1).

17 *Palynological preparations and analyses*

18 Palynological analyses were performed at 8 cm intervals with a volume of $\sim 5 \text{ cm}^3$ of wet sediment
19 following the protocol described by Rochon *et al.* (1999). Marker grains (*Lycopodium clavatum*
20 spore tablets, batch n°414831, Lund University) were added in each sample to estimate
21 palynomorph concentrations following the method described by Matthews (1969) and Mertens *et*
22 *al.* (2009). The concentrations (cysts cm^{-3}) were multiplied by the sedimentation rate (cm yr^{-1}) in
23 each sample in order to describe the abundances as influxes ($\text{cysts cm}^{-2} \text{ yr}^{-1}$). This makes it easier

1 to assess changes in dinoflagellate and benthic (organic linings of foraminifera) productivities in
2 environments where sedimentation rates vary through time. After wet sieving the samples at 100
3 and 10 μm to eliminate sand, fine silt and clay, the 10-100 μm fraction was chemically treated with
4 hydrochloric (HCl, 10%) to eliminate carbonates and hydrofluoric acids (HF, 49%) to eliminate
5 silicates. The residual organic matter was mounted on microscope slides with glycerin gelatin, and
6 slides were analyzed using a transmitted light microscope at magnifications of 400x to 1000x.
7 Dinocysts and organic linings of foraminifera were identified and counted (Fig. 2) until reaching a
8 minimum of 300 dinocysts and 100 marker-grains in each sample. Reworked and freshwater
9 palynomorphs were also counted. Organic linings of foraminifera observed in the samples are
10 mainly benthic, as they are more resistant to dissolution than those of planktic foraminifera (de
11 Vernal *et al.*, 1992). The identification of dinocyst followed the nomenclature provided by Rochon
12 *et al.* (1999), Head *et al.* (2001), Radi *et al.* (2013), Mertens *et al.* (2018) and Londeix *et al.* (2018).

13 *Statistical approach and data analyses*

14 The modern analogue technique (MAT) allowed to reconstruct sea surface conditions using a
15 dinocyst database of the Northern Hemisphere that includes 1776 reference sites and 73 taxa (Allan
16 *et al.*, 2018). The calculations were performed using the Bioindic scripts developed for the R
17 platform by Joel Guiot (CEREGE, France) and the procedure described by de Vernal *et al.* (2013b).
18 The MAT relies on the hypothesis that similar biogenic assemblages occur under similar
19 environmental conditions without any assumptions in terms of quantitative relationships (Guiot
20 and de Vernal, 2007). Although there have been some concerns expressed that root mean square
21 error of prediction (RMSEP) might be underestimated (Telford, 2006; Telford and Birks, 2005,
22 2011), this method (MAT) has been demonstrated as reliable as any reconstruction method using
23 micropaleontological proxies (Guiot and de Vernal, 2011).

1 Five analogues were used, and a logarithmic transformation was applied on the relative abundance
2 of dinocysts for the reconstructions. The errors of prediction on winter and summer SSTs are
3 $\pm 1.4/1.7^{\circ}\text{C}$, and $\pm 1.2/2.1$ for SSSs. SIC extent is expressed in number of months with more than
4 50% ice coverage (based on the 1953-2003 mean) (± 1.4 months/year) and productivity in gC m^{-2}
5 yr^{-1} (± 61.5 $\text{gC m}^{-2} \text{yr}^{-1}$). The Heterotrophic/Autotrophic (H/A) dinocysts ratio was calculated to
6 assess temporal changes in the dominant trophic mode. Finally, principal component analyses
7 (PCA) were performed with the software PAST (Hammer *et al.*, 2001) to differentiate the
8 distribution of assemblages (taxa $< 1\%$ were excluded).

9 **Results**

10 The two cores used in this study (204 and Kane2B) were described in detail by Caron *et al.* (2019)
11 and Georgiadis *et al.* (2018) and major sedimentological units (Fig. S1) were distinguished based
12 on lithology and physical property of the sediment. Overall, the lithology of core 204 is relatively
13 homogeneous and fine grained and is largely dominated by hemipelagic sedimentation. At the
14 opposite, core Kane2B is showing a more variable sedimentation associated to higher inputs of ice-
15 rafted debris (IRD) and reworked sediments throughout the core (Caron *et al.*, 2019; Georgiadis *et*
16 *al.*, 2018). Palynological results provide additional details on environmental changes for both cores.
17 A total of 25 dinocyst taxa were identified, 14 of which account for more than 95 % of the
18 assemblages (Table 2 and Fig. 2). One interval at the base of core Kane2B (428-300 cm, ca. 9000-
19 8300 cal a BP) was not considered for palynological reconstructions due to very low dinocyst
20 concentrations. Relative abundance of the main taxa accounting for more than 95 % of the
21 assemblages are presented in Figs. 3 and 5. Main dinocyst assemblage zones were distinguished
22 based on the scores of the first two components of the PCA (Fig. S2), reflecting the occurrence of
23 accompanying taxa and changes in abundance of the dominant species. Reconstructions of sea-

1 surface properties including SST, SSS, SIC and primary productivity are shown in Figs. 4 and 6,
2 together with organic linings of foraminifera, freshwater (*Halodinium*) and reworked palynomorph
3 influxes. The reconstructed primary productivity represents the productivity of all autotrophic
4 groups (including diatoms, ciliates, etc.; e.g., Cormier *et al.*, 2016).

5 *AMD14-204 – Northwestern Greenland margin*

6 Dinocyst assemblages were recovered from all samples in core 204, with an average estimated flux
7 of 1260 ± 100 cysts $\text{cm}^{-2} \text{yr}^{-1}$, and a maximum value of 4830 cysts $\text{cm}^{-2} \text{yr}^{-1}$ between ca. 5700 and
8 5600 cal a BP (Fig. 3). Overall, reconstructed SST ranged from -1.7 to 7°C , summer SSS ranged
9 from 27 to 32.8, SIC between 3 and 9 months per year and primary productivity between 90 and
10 $190 \text{ gC m}^{-2} \text{yr}^{-1}$ (Fig. 4). The characteristics of each dinocyst assemblage zone are described below
11 in terms of relative abundance and sea-surface conditions reconstructions:

12 **Zone 1** (prior to 7750 cal a BP; 738- 604 cm) is characterized by the dominance of heterotrophic
13 taxa, such as *Islandinium minutum* (up to 39 %) and *Brigantedinium* spp. (up to 46 %), as revealed
14 by the H/A ratio (Fig. 4). It is also characterized by the highest relative abundances of
15 *Impagidinium pallidum* (up to 4 %), and *Polykrikos* var. Arctic (up to 3.5 %), which nearly
16 disappears after 7750 cal a BP (Fig. 3). Sea-surface reconstructions reveal the lowest SST values
17 (summer SST averaging $\sim 2^\circ\text{C}$) and the maximum SIC duration (8-9 months/year) of the entire core
18 (Fig. 4).

19 **Zone 2** (7750-3350 cal a BP; 604-164 cm) is dominated by “warmer water” autotrophic species
20 (Rochon *et al.*, 1999; Zonneveld *et al.*, 2013), including *Operculodinium centrocarpum* and
21 *Spiniferites elongatus*, and by the gradual increase of the cyst of *Pentapharsodinium dalei* (from
22 ~ 7 to 37 %). The dominance of these autotrophic species after 7750 cal a BP is reflected by the
23 low H/A ratio (Fig. 4). Assemblage zone 2 was sub-divided into 5 sub-zones, which coincide with

1 the maximum (sub-zones 2a, 2c and 2e) and minimum (sub-zones 2b and 2d) relative abundance
2 of *O. centrocarpum* (Figs. 3 and S2). Sub-zone 2a (7750-6880 cal a BP; 604-521 cm) is
3 characterized by the sharp increase of *O. centrocarpum*, *S. elongatus* and *Spiniferites ramosus*, the
4 decrease of *I. minutum* and *Brigantedinium* spp. and near disappearance of *Polykrikos* var. Arctic.
5 The transition between sub-zones 2a and 2b (6880-6450 cal a BP; 521-475 cm) is marked by the
6 arrival of *N. labyrinthus*, the low abundance of *O. centrocarpum* and the increase of heterotrophic
7 taxa (*Echinidinium karaense*, *I. minutum* and *Brigantedinium* spp.; Fig. 3). Sub-zone 2c (6450-
8 5100 cal a BP; 475-300 cm) corresponds to the highest abundance of *O. centrocarpum* (up to 67
9 %), *S. elongatus* (up to 18 %) and *S. ramosus*, and low abundance of all heterotrophic taxa (Fig.
10 3). It is also characterized by the highest production of organic linings of foraminifera (up to 1500
11 linings cm⁻² yr⁻¹; Fig. 4). Sub-zone 2d (5100-4750 cal a BP; 300-282 cm) is characterized by the
12 maximum abundance of *E. karaense* and sharp decrease of the gonyaulacacean taxa (*O.*
13 *centrocarpum*, *S. ramosus*, *S. elongatus* and *N. labyrinthus*; Fig. 3). Finally, sub-zone 2e (4750-
14 3350 cal a BP; 282-164 cm) is characterized by another increase in the abundance of
15 Gonyaulacacean taxa. Overall, reconstructed SST, SSS and primary productivity conditions
16 display a series of 3 pulses of high SST values (sub-zones 2a, 2c and 2e), alternating with 2 short
17 periods of low values (sub-zones 2b and 2d) (Fig. 4). The 3 “warm” pulses are marked by relatively
18 low SIC duration, while the cooler periods are marked by increased SIC, up to 9 months/yr (Fig.
19 4).

20 **Zone 3** (3350-700 cal a BP; 164-0 cm) is characterized by the maximum abundance of both the
21 cyst of *P. dalei* (up to 71 %; Fig. 3) and *N. labyrinthus*. It is subdivided into two sub-zones. Sub-
22 zone 3a (3350-2170 cal a BP; 164-106 cm) is dominated by the cyst of *P. dalei* (avg. ~55%), a
23 decrease of *O. centrocarpum* abundance, relatively stable values of the other “North Atlantic” taxa

1 (*S. elongatus*, *N. labyrinthus* and *S. ramosus*), and slightly increasing abundances of *I. minutum*
2 and *E. karaense*. Sub-zone 3b (2170-700 cal a BP; 106-0 cm) is characterized by the maximal
3 abundance of cyst of *P. dalei*, an increase of *O. centrocarpum* and a peak in the abundance of *N.*
4 *labyrinthus*. All heterotrophic taxa are at their lowest abundance in this sub-zone. Sea-surface
5 reconstructions for Zone 3 indicate the highest SST and primary productivity values throughout
6 the core, as well as the lowest values of SIC (Fig. 4).

7 *AMD14-Kane2B – Kane Basin*

8 Dinocysts are less abundant in core Kane2B compared to core 204 and influxes range from
9 extremely low (barren in dinocyst at the base) to 397 cysts $\text{cm}^{-2} \text{yr}^{-1}$, with maximum values recorded
10 between 4500 and 3000 cal a BP (Fig. 5). Maximum influxes of foraminiferal linings (up to 500
11 linings $\text{cm}^{-2} \text{yr}^{-1}$) are recorded between 8100 and 7400 cal a BP (Fig. 6), suggesting higher benthic
12 productivity. Reworked palynomorphs are abundant throughout the core (up to 1200 cells $\text{cm}^{-2} \text{yr}^{-1}$
13 at the base of the core, Fig. 6), which suggests high erosion and remobilization of pre-Quaternary
14 sediments. The core is largely dominated by heterotrophic taxa (77-100 %) as reflected by the A/H
15 ratio < 1 (Fig. 6). Overall, reconstructed SST ranged from -1.8 to 2.2°C, summer SSS ranged from
16 27 to 33, SIC between 8 and 10 months per year, and primary productivity between 55 and 120 gC
17 $\text{m}^{-2} \text{yr}^{-1}$.

18 **Zone 1:** Prior to 8300 cal a BP (427-298 cm), dinocyst abundance was too low to achieve
19 reconstructions. Nonetheless, the few specimens found were mostly of *Brigantedinium* spp., *E.*
20 *karaense* and *I. minutum*, suggesting harsh sea-surface conditions, likely associated with a
21 perennial or quasi-perennial SIC. A peak of dinocyst influx at 8100 cal a BP is associated to an
22 increase of *E. karaense* (up to 45 %) and a slight decrease of *Brigantedinium* spp. (Fig. 5).

1 **Zone 2** (7880-5200 cal a BP; 270-172 cm) is marked by maximum abundances of autotrophic
2 species (*O. centrocarpum* and *S. elongatus*), although the assemblage remains dominated by
3 heterotrophic taxa, such as *Brigantedinium* spp., *E. karaense* and *I. minutum* (Fig. 5 and A/H ratio,
4 Fig. 6). It is subdivided into two sub-zones based on the relative abundances of taxa. Sub-zone 2a
5 (7880-7225 cal a BP; 270-242 cm) is marked by low dinocyst influxes (~ 60 cysts $\text{cm}^{-2} \text{yr}^{-1}$) and
6 the appearance of the cyst of *P. dalei*. It is dominated by *Brigantedinium* spp. and accompanied by
7 *I. minutum*, but it also corresponds to the maximal abundance of *O. centrocarpum* (up to 11 %), *S.*
8 *elongatus* (up to 4 %) and *I. pallidum* (up to 2 %). Sea surface reconstructions indicate maximum
9 values of summer SST and SSS during this period. Sub-zone 2b (7225-5200 cal a BP; 242-172 cm)
10 is dominated by *E. karaense* (up to 49 %) and *I. minutum* (up to 41 %). It is also characterized by
11 the highest relative abundance of *Polykrikos* var. Arctic (up to 5 %), an Arctic species restricted to
12 regions characterized by cold surface waters (Zonneveld *et al.*, 2013). Sea surface reconstruction
13 revealed relatively low summer SST ($\sim 1^\circ\text{C}$), SSS (~ 27 psu) and primary productivity (~ 60 gC m^{-2}
14 yr^{-1}), and an extended SIC during this period (Fig. 6).

15 **Zone 3** (5200 cal a BP to present; 172-0 cm) is characterized by *Brigantedinium* spp. and a
16 progressive increase of the relative abundance of *I. minutum* (20 to 47 %). A change occurred
17 around ca. 2100 cal a BP, which leads to the subdivision into 2 sub-zones. Sub-zone 3a (5200-2100
18 cal a BP; 172-45 cm) is characterized by the maximum relative abundance of *Brigantedinium* spp.
19 (up to 57 %), low abundance of *E. karaense* (~ 15 %), and maximum dinocyst influxes (4500 to
20 3000 cal a BP). Sub-zone 3b (2100 cal a BP to present; 45-0 cm) is characterized by the maximum
21 abundance of *I. minutum* (up to 48 %) and by increasing abundances of *E. karaense*, *Polykrikos*
22 var. Arctic and cyst of *P. dalei* (Fig. 5). Sea-surface reconstructions reveal a slight increase in SIC
23 and a slight decrease in SST and primary productivity during this period (Sub-zone 3b, Fig. 6).

1 **Discussion**

2 Dinocyst assemblages from two sites (204 and Kane2B) reflect important oceanographic
3 changes throughout the Holocene. The results indicate a shift from cold and extended SIC to milder
4 postglacial conditions with seasonal SIC that occurred around 7880 cal a BP in the Kane Basin and
5 around 7750 cal a BP in the northeast Baffin Bay. The synthesis on the timing of climatic and
6 environmental changes documented from both cores are presented on Figs. 7 and 8. Results from
7 core 204 (Fig. 7) are compared with regional record from Disko Bugt (MSM343300: Ouellet-
8 Bernier *et al.*, 2014), while results from core Kane2B (Fig. 8) are compared with regional records
9 from Smith Sound (Sites 008 and 012: Levac *et al.*, 2001) and Lancaster Sound (2004-804-009:
10 Ledu *et al.*, 2008).

11 *Early Holocene - End of deglaciation*

12 In both cores, assemblages from this period (prior to 7750 and 7880 cal a BP, respectively) are
13 dominated by *Brigantedinium* spp., *I. minutum*, *E. karaense* and accompanied by *Polykrikos* var.
14 Arctic. The co-dominance of those taxa is often associated with harsh, densely ice-covered
15 conditions and relatively high productivity (de Vernal *et al.*, 2001, 2013a; Head *et al.*, 2001;
16 Rochon *et al.*, 1999; Zonneveld *et al.*, 2013). Low dinocyst influxes and the dominance of these
17 heterotrophic species suggest primary productivity probably dominated by diatoms, which
18 constitute the main food source of heterotrophic dinoflagellates (e.g., Jacobson and Anderson,
19 1986). Diatoms are usually advantaged (opportunists) compared to dinoflagellates in areas where
20 nutrients are relatively abundant (e.g., Dale, 1996; Lovejoy *et al.*, 2002).

21 At the site of core 204, the sea surface reconstructions revealed the lowest SST values (~2°C in
22 summer, ~-1.4°C in winter) and the highest SIC duration (up to 9 months/year) during this period,
23 although associated to minimal values of productivity (Fig. 4). Harsh sea-surface conditions likely

1 prevented the development of phototrophic dinocysts taxa in this area, while primary producers
2 such as diatoms may account for the presence of heterotrophic dinocysts taxa. Previous studies
3 (e.g., Ouellet-Bernier *et al.*, 2014; Gibb *et al.*, 2015) in the region of Disko Bugt have also observed
4 dinocyst assemblages dominated by heterotrophic taxa prior to 7300 and 7400 cal a BP
5 respectively. Besides, Jennings *et al.* (2014) determined a continuous GIS mass loss until 7800 cal
6 a BP based on foraminifera and other proxies. Thus, the relatively low reconstructed salinity values
7 in core 204 support evidence of high meltwater discharge from the GIS prior to 7750 cal a BP, also
8 suggested in Caron *et al.* (2019).

9 In Kane Basin, immediately after the retreat of grounded ice from the core site, the high
10 concentration of reworked palynomorphs (Fig. 6) associated to a high IRD content support ice-
11 proximal conditions with high meltwater discharge from both IIS and GIS (Caron *et al.*, 2019;
12 Georgiadis *et al.*, 2018). This strong meltwater input, linked to the retreating ice sheets, probably
13 resulted in very harsh sea surface conditions with a quasi-permanent SIC during this period (prior
14 to 8300 cal a BP; Ledu *et al.*, 2010), which would explain the very low concentration of dinocysts
15 observed during this period. Moreover, we consider that this period before 8300 cal a BP is linked
16 to a major oceanographic reorganization associated with the opening of Nares Strait and
17 establishment of the modern oceanic circulation (e.g., Jennings *et al.*, 2011, 2019; Georgiadis *et*
18 *al.*, 2018).

19 *Onset of full interglacial conditions*

20 On the Northwestern Greenland margin (core 204), a major shift is recorded around 7750 cal a
21 BP, representing a change in dominant species from heterotrophic to phototrophic taxa. It was also
22 associated with a rapid increase of dinocyst influxes and species richness, hence suggesting milder
23 conditions with warmer SST and a reduced SIC during this period (Figs. 3 and 7). Several regional

1 records (based on dinocysts or foraminifera) have also observed a major shift due to surface and
2 subsurface warming occurring between 7400-7800 cal a BP, which is considered as the transition
3 towards modern postglacial conditions and warmer sea-surface conditions (e.g., Perner *et al.*, 2013;
4 Ouellet-Bernier *et al.*, 2014; Jennings *et al.*, 2014; Gibb *et al.*, 2015). Indeed, the establishment of
5 warmer conditions in Baffin Bay is likely a response to the reinforcement of the warm and saline
6 component (IC) of the WGC, linked with the final retreat of both LIS and GIS (Lloyd *et al.*, 2005;
7 Ouellet-Bernier *et al.*, 2014; Gibb *et al.*, 2015). In addition, the dominance of the phototrophic
8 species *O. centrocarpum* and *S. elongatus* is often associated with the North Atlantic Drift,
9 suggesting surface water temperatures $> 0^{\circ}\text{C}$ throughout the year (Rochon *et al.*, 1999; Mudie *et*
10 *al.*, 2006; Zonneveld *et al.*, 2013).

11 In Kane Basin, this transition towards interglacial conditions is also marked by the increase of
12 accompanying autotrophic species *O. centrocarpum* and *S. elongatus* from 7880 to 7200 cal a BP,
13 although the assemblage is still dominated by heterotrophic taxa (Fig. 5). This suggests warmer
14 sea-surface conditions, which nonetheless remained relatively cold with an extended SIC, as
15 expected considering the presence of the strong cold Arctic current flowing southwards in the basin
16 (Münchow *et al.*, 2006). This is coherent with Levac *et al.* (2001), whom suggest sea-surface
17 temperatures up to 3°C higher than at present as early as 7800 ^{14}C a BP (~ 8000 cal a BP) in Smith
18 Sound (Fig. 8). As *O. centrocarpum* and *S. elongatus* are considered as Atlantic water indicators,
19 these results could reflect the entry of warmer Atlantic water into the basin (via the IC) associated
20 with the enhanced strength of the WGC during this period (Perner *et al.*, 2013), the insolation
21 maximum (Lecavalier *et al.*, 2017) and isostatic readjustment after the retreat of grounded ice
22 (England *et al.*, 2006).

1 *Middle Holocene - Holocene Thermal Maximum*

2 Dinocyst assemblages of core 204 indicate that warm postglacial conditions were established in
3 northeastern Baffin Bay after 7750 cal a BP, although two periods (6880-6450 and 5100-4750 cal
4 a BP) are marked by the decrease of *O. centrocarpum* abundance (warm water taxa) and increase
5 of the abundance of *E. karaense* and *I. minutum* (cold taxa; Fig. 3). These two periods are associated
6 with relatively lower reconstructed SST and productivity values and a higher SIC duration (Fig. 4).
7 These results suggest a temporary return to colder sea-surface conditions during these periods,
8 possibly caused by meltwater pulses from the GIS, also evidenced by moderate peak abundance of
9 *Halodinium* sp. at the top of both sub-zones. Overall, we associate the period from 7750 to 3350
10 cal a BP to the Holocene Thermal Maximum (HTM), with optimal conditions observed between
11 6400 and 5500 cal a BP (Fig. 7). The high dinocyst influx, as well as the relatively high
12 reconstructed SST and productivity values support this interpretation (Figs. 4 and 7), which is also
13 consistent with previous regional works (e.g., Ouellet-Bernier *et al.*, 2014; Jennings *et al.*, 2014).
14 Furthermore, a higher influence of the IC (stronger, saltier and warmer WGC) was recorded
15 between 6200 and 3500 a BP by Perner *et al.* (2013).

16 As mentioned above, our data from Kane Basin suggest warmer conditions between 7880 and
17 7200 cal a BP, with the highest relative abundance of 'North Atlantic' indicators. This period is
18 also characterized by maximum influxes of foraminiferal linings (high benthic productivity) and
19 very low dinocyst influxes (Fig. 8). Regional studies (Bradley, 1990; Levac *et al.*, 2001; Knudsen
20 *et al.*, 2008; Jennings *et al.*, 2011; Lecavalier *et al.*, 2017) have recorded an early HTM in this area
21 compared to lower latitudes sites (e.g., Disko Bugt or Labrador Sea). Likewise, Ledu *et al.* (2010)
22 observed an increase of the phototrophic taxa relative abundance, linked with the HTM between
23 8500 and 5500 cal a BP. Nevertheless, the low dinocyst influxes and high benthic productivity

1 suggest that dinoflagellates may not be solely responsible for the primary productivity in the Nares
2 Strait area, and that diatoms may be involved (Cormier *et al.*, 2016). Thus, our results could reflect
3 relatively open water conditions without ice arch formation during this period, favorable for the
4 development of phototrophic dinocysts species and diatoms.

5 *Late Holocene changes in sea surface conditions*

6 Regionally, the Late Holocene is characterized by a cooling trend which corresponds to the
7 Neoglacial period associated with glacier growth and subsurface cooling along the West Greenland
8 coast (e.g., Briner *et al.*, 2016; Perner *et al.*, 2013; Schweinsberg *et al.*, 2017). This neoglacial
9 cooling period is recorded over the last ca. 4000 cal a BP in regional reconstructions (e.g., Knudsen
10 *et al.*, 2008; Seidenkrantz *et al.*, 2008; Krawczyk *et al.*, 2010; Andresen *et al.*, 2010). The
11 fluctuations observed in the reconstructed sea-surface conditions at both our sites over the last ca.
12 3500 cal a BP reflect this cooling to a certain extent after ~2000 cal a BP.

13 However, after 3350 cal a BP, core 204 is marked by a major change in the dinocyst assemblages
14 with a dominance shift from *O. centrocarpum* to cyst of *P. dalei* (Fig. 3), suggesting changes in
15 surface water conditions during this period, which were not observed in other regional dinocyst
16 records (e.g., Ouellet-Bernier *et al.*, 2014; Gibb *et al.*, 2015). In the Arctic, cysts of *P. dalei* are
17 associated with relatively warm, stratified and highly productive waters, and generally require SST
18 higher than 4°C (Rochon *et al.*, 1999; Matthiessen *et al.*, 2005; Ribeiro *et al.*, 2012). Moreover,
19 high abundances of cysts of *P. dalei* are recorded in location with large seasonal temperature
20 gradient (Rochon *et al.*, 1999). Thus, the dominance of this species, which is found in abundance
21 near Iceland (Zonneveld *et al.*, 2013) could reflect a higher seasonal gradient during this period,
22 possibly from an increased contribution of the Atlantic component (IC) to the WGC. Indeed,

1 warmer SST (increase by $\sim 1.5^{\circ}\text{C}$) after ~ 3.1 cal ka BP were also observed by Gibb *et al.* (2015)
2 and was attributed to an enhanced strength of the IC.

3 Reconstructions from Kane Basin reflect the abundance of the dominant taxa: *Brigantedinium*
4 spp. for the productivity and SST, and *I. minutum*+*E. karaense* for the SIC duration. We interpret
5 the maximum dinocyst influxes and dominance of *Brigantedinium* spp. between 5200 and 2100 cal
6 a BP to reflect an increased primary productivity linked to the availability of pelagic prey, mostly
7 diatoms (Jacobson and Anderson, 1986; Matthiessen *et al.*, 2005; Cormier *et al.*, 2016), but not
8 necessarily warmer conditions. Besides, we associate the increasing trend of *I. minutum* after 5200
9 cal a BP to a progressive cooling, possibly linked to the Neoglaciation. This cooling trend
10 intensified over the last 2100 cal a BP (increase of *I. minutum*, *E. karaense* and *Polykrikos* var.
11 Arctic) with decreasing dinocyst influxes (Figs. 5 and 8). Indeed, the relative abundance of *I.*
12 *minutum* increases linearly with the duration of seasonal SIC in Arctic regions (Zonneveld *et al.*,
13 2013). This is coherent with the work of Levac *et al.* (2001) that observed a general deterioration
14 of sea-surface conditions over the last ~ 3200 cal a BP in Smith Sound (increased SIC; Fig. 8).
15 Finally, Ledu *et al.* (2008) also recorded a cooling trend in Lancaster Sound starting after 5500 cal
16 a BP. Thus, we suggest that the increase of *I. minutum* and *E. karaense* observed at the top of core
17 (last 2100 cal a BP) could reflect this regional cooling trend of the late Holocene.

18 **Conclusions**

19 Paleoclimatic reconstructions based on dinocyst assemblages from two sediment cores
20 (AMD14-204 and AMD14-Kane2B) using the MAT provided insight on the evolution of sea-
21 surface conditions during the Holocene. In the northeastern Baffin Bay (core 204), the dinocyst
22 assemblages revealed important changes throughout the Holocene, with harsh conditions prior to
23 7750 cal a BP, associated to an extended SIC and high meltwater inputs from the retreating GIS.

1 A shift to warmer conditions occurred around 7750 cal a BP, as a response to the final retreat of
2 the GIS and a strengthened North Atlantic component (IC) of the WGC. From 7750 to 3350 cal a
3 BP, the dominance of phototrophic taxa and highest species richness marks the mid-Holocene
4 thermal optimum associated with warmer SST, higher productivity and reduced SIC, culminating
5 between 6450 and 5100 cal a BP. Finally, after 3350 cal a BP, the progressive establishment of
6 modern dinocyst assemblages is observed, associated with higher seasonality.

7 In Kane Basin (core Kane2B), our results revealed the dominance of heterotrophic taxa
8 throughout the core. Results suggest relatively cold sea-surface conditions, with abundant SIC
9 during most of the Holocene in this area. Nonetheless, variations of the dinocyst assemblages reveal
10 some changes in the sea-surface conditions following the opening of Nares Strait (and the
11 strengthened southward flow of cold Arctic water through Nares Strait). Enhanced contribution of
12 Atlantic water recorded between 7880 and 7200 cal a BP, marked by the occurrence of autotrophic
13 taxa, suggest oceanographic conditions different than present, likely caused by the insolation
14 maximum and breakup of the IIS. Maximum primary productivity recorded between 5200 and
15 2100 cal a BP reflects the availability of prey for heterotrophic dinoflagellates. Finally, an
16 increasing abundance of the Arctic taxa *I. minutum* is associated with a progressive cooling trend,
17 which intensified after 2100 cal a BP.

18 Overall, this study indicates that sea-surface conditions in northeastern Baffin Bay are more
19 favorable for the growth of autotrophic dinoflagellates than in Nares Strait. This is explained by
20 the influence of the warm and relatively salty WGC on the eastern side of Baffin Bay compared to
21 the strong southward Arctic flow in Nares Strait. Finally, this study confirmed the important
22 changes in sea-surface conditions that occurred from the end of the deglaciation until present, both
23 for the Northwestern Greenland shelf and Nares Strait. These variations can be associated to

1 changes in meltwater discharges or varying strength of oceanic currents (e.g., IC or EGC influence)
2 themselves related to the main climatic changes of the Holocene.

3
4 *Abbreviations.* BIC, Baffin Island Current; CAA, Canadian Arctic Archipelago; EGC, East Greenland
5 Current; GIS, Greenland Ice Sheet; HTM, Holocene Thermal Maximum; IC, Irminger Current; IIS,
6 Innuitian Ice Sheet; IRD, ice-rafted debris; LGM, Last Glacial Maximum; LIS, Laurentide Ice Sheet; MAT,
7 modern analogue technique; RDL, rapidly-deposited layer; SIC, Sea-ice cover; SST, Sea-surface
8 temperature; SSS, Sea-surface salinity; WGC, West Greenland Current.

9 **References**

- 10 Aksu AE, Piper DJW. 1987. Late Quaternary sedimentation in Baffin Bay. *Canadian Journal of Earth*
11 *Science* **24**: 1833–1846.
- 12 Allan E, de Vernal A, Knudsen MF, *et al.* 2018. Late Holocene Sea Surface Instabilities in the Disko Bugt
13 Area, West Greenland, in Phase With $\delta^{18}\text{O}$ Oscillations at Camp Century. *Paleoceanography and*
14 *Paleoclimatology* **33**: 227–243.
- 15 Andresen CS, McCarthy DJ, Valdemar Dylmer C, *et al.* 2010. Interaction between subsurface ocean waters
16 and calving of the Jakobshavn Isbrae during the late Holocene. *The Holocene* **21**: 211–224.
- 17 Barber DG, Hanesiak JM, Chan W, *et al.* 2001. Sea-ice and meteorological conditions in Northern Baffin
18 Bay and the North Water polynya between 1979 and 1996. *Atmosphere-Ocean* **39**(3): 343-359.
- 19 Bradley RS. 1990. Holocene paleoclimatology of the Queen Elizabeth Islands, Canadian High Arctic.
20 *Quaternary Science Reviews* **9**(4): 365-384.
- 21 Briner JP, McKay NP, Axford Y, *et al.* 2016. Holocene climate change in Arctic Canada and Greenland.
22 *Quaternary Science Reviews* **147**: 340-364.
- 23 Caron M, St-Onge G, Montero-Serrano JC, *et al.* 2019. Holocene chronostratigraphy of northeastern Baffin
24 Bay based on radiocarbon and paleomagnetic data. *Boreas*.
- 25 Cormier MA, Rochon A, de Vernal A, *et al.* 2016. Multi-proxy study of primary production and
26 paleoceanographical conditions in northern Baffin Bay during the last centuries. *Marine*
27 *Micropaleontology* **127**: 1-10.
- 28 Dale B. 1996. Dinoflagellate cyst ecology: modelling and geological applications. In: Jansonius, J.,
29 Gregory, C.D. (Eds.), *Palynology: Principles and Applications*. The American Association of
30 Stratigraphic Palynologists Foundation, Salt Lake City : Publishers Press, Salt Lake City, pp. 1249–1276
- 31 de Vernal A, Bilodeau G, Hillaire-Marcel C, *et al.* 1992. Quantitative assessment of carbonate dissolution
32 in marine sediments from foraminifer linings vs. shell ratios: Davis Strait, northwest North Atlantic.
33 *Geology* **20**(6): 527-530.

- 1 de Vernal A, Henry M, Matthiessen J, *et al.* 2001. Dinoflagellate cyst assemblages as tracers of sea-surface
2 conditions in the Northern North Atlantic, Arctic and sub-Arctic seas: The new “n = 677” data base and
3 its application for quantitative palaeoceanographic reconstruction. *Journal of Quaternary Science* **16**:
4 681–698.
- 5 de Vernal A, Hillaire-Marcel C, Rochon A, *et al.* 2013a Dinocyst-based reconstructions of sea ice cover
6 concentration during the Holocene in the Arctic Ocean, the northern North Atlantic Ocean and its
7 adjacent seas. *Quaternary Science Review* **79**: 111–121.
- 8 de Vernal A, Rochon A, Fréchette B, *et al.*, 2013b. Reconstructing past sea ice cover of the Northern
9 Hemisphere from dinocyst assemblages: Status of the approach. *Quaternary Science Reviews* **79**: 122–
10 134.
- 11 England JH, Atkinson N, Bednarski J, *et al.* 2006. The Innuitian Ice Sheet: configuration, dynamics and
12 chronology. *Quaternary Science Review* **25**: 689–703.
- 13 Fensome RA, Taylor FJR, Norris G, *et al.* 1993. A classification of living and fossil dinoflagellates.
14 *Micropaleontology, Special Publication* **7**.
- 15 Georgiadis E, Giraudeau J, Martinez P, *et al.* 2018. Deglacial to postglacial history of Nares Strait,
16 Northwest Greenland: a marine perspective. *Climate of the past*. doi.org/10.5194/cp-2018-78
- 17 Gibb OT, Steinhauer S, Frechette B, *et al.* 2015. Diachronous evolution of sea surface conditions in the
18 Labrador Sea and Baffin Bay since the last deglaciation. *The Holocene* **25**: 1882–1897.
- 19 Giraudeau J, Georgiadis E, Caron M, *et al.* under review. A high-resolution elemental record of post-glacial
20 lithic sedimentation in Upernavik Trough, western Greenland: history of ice-sheet dynamics and ocean
21 circulation changes over the last 9 100 years. *Global and planetary change*.
- 22 Guiot J, de Vernal A. 2007. Transfer functions: methods for quantitative paleoceanography based on
23 microfossils. In Proxies in Late Cenozoic Paleoceanography. *Developments in Marine Geology*, Hillaire-
24 Marcel C, de Vernal A (eds). Elsevier: Amsterdam; 523–563.
- 25 Guiot J, de Vernal A. 2011. QSR Correspondence “Is spatial autocorrelation introducing biases in the
26 apparent accuracy of palaeoclimatic reconstructions?” Reply to Telford and Birks. *Quaternary Science*
27 *Reviews* **21**(30): 3214-3216.
- 28 Hammer Ø, Harper DAT, Ryan PD, 2001. PAST: Paleontological Statistics Software Package for Education
29 and Data Analysis. *Palaeontologia Electronica* **4**(1): 9pp.
- 30 Head MJ, Harland R, Matthiessen J. 2001. Cold marine indicators of the late Quaternary: The new
31 dinoflagellate cyst genus *Islandinium* and related morphotypes. *Journal of Quaternary Science* **16**: 621–
32 636.
- 33 Jacobson DJ, Anderson, DM. 1986. Thecate heterotrophic dinoflagellates: feeding behavior and
34 mechanisms. *Journal of Phycology* **22**: 249-258.
- 35 Jakobsson M, Long AJ, Ingólfsson Ó, *et al.* 2010. New insights on Arctic Quaternary climate variability
36 from palaeo-records and numerical modelling. *Quaternary Science Review* **29**: 3349–3358.
- 37 Jennings AE, Sheldon C, Cronin T, *et al.* 2011. The Holocene History of Nares Strait: Transition from
38 Glacial Bay to Arctic-Atlantic Throughflow. *Oceanography* **24**: 26–41.

- 1 Jennings AE, Walton ME, Ó Cofaigh C, *et al.* 2014. Paleoenvironments during Younger Dryas-Early
2 Holocene retreat of the Greenland Ice Sheet from outer Disko Trough, central west Greenland. *Journal*
3 *of Quaternary Science* **29**(1): 27-40.
- 4 Jennings AE, Andrews JT, Oliver B, *et al.* 2019. Retreat of the Smith Sound Ice Stream in the Early
5 Holocene. *Boreas*.
- 6 Knudsen KL, Stabell B, Seidenkrantz MS, *et al.* 2008. Deglacial and Holocene conditions in northernmost
7 Baffin Bay: Sediments, foraminifera, diatoms and stable isotopes. *Boreas* **37**: 346–376.
- 8 Krawczyk D, Witkowski A, Moros M, *et al.* 2010. Late-Holocene diatom-inferred reconstruction of
9 temperature variations of the West Greenland Current from Disko Bugt, central West Greenland. *The*
10 *Holocene* **20**: 659–666.
- 11 Krawczyk D, Witkowski A, Moros M, *et al.* 2017. Quantitative reconstruction of Holocene sea ice and sea
12 surface temperature off West Greenland from the first regional diatom data set. *Paleoceanography* **32**:
13 18–40.
- 14 Kwok R, Toudal Pedersen L, Gudmandsen P, & Pang SS, 2010. Large sea ice outflow into the Nares Strait
15 in 2007. *Geophysical Research Letters* **37**(3).
- 16 Lecavalier BS, Fisher DA, Milne GA, *et al.* 2017. High Arctic Holocene temperature record from the
17 Agassiz ice cap and Greenland ice sheet evolution. *Proceedings of the National Academy of Sciences*
18 **114**(23): 5952-5957.
- 19 Ledu D, Rochon A, de Vernal A *et al.* 2008. Palynological evidence of Holocene climate change in the
20 eastern Arctic: A possible shift in the Arctic oscillation at the millennial time scale. *Canadian Journal*
21 *of Earth Science* **45**: 1363–1375.
- 22 Ledu D, Rochon A, de Vernal A, *et al.* 2010. Holocene paleoceanography of the northwest passage,
23 Canadian Arctic Archipelago. *Quaternary Science Reviews* **29**(25-26): 3468-3488.
- 24 Levac E, de Vernal A, Blake WJ, 2001. Sea-surface conditions in northernmost Baffin Bay during the
25 Holocene: Palynological evidence. *Journal of Quaternary Science* **16**: 353–363.
- 26 Lloyd JM, Park LA, Kuijpers A, *et al.* 2005. Early Holocene palaeoceanography and deglacial chronology
27 of Disko Bugt, west Greenland. *Quaternary Science Reviews* **24**(14-15): 1741-1755.
- 28 Londeix L, Zonneveld K, Masure E. 2018. Taxonomy and operational identification of Quaternary species
29 of *Spiniferites* and related genera. *Palynology*, **42**(sup1): 45-71.
- 30 Lovejoy C, Legendre L, Martineau MJ, *et al.* 2002. Distribution of phytoplankton and other protists in the
31 North Water. *Deep Sea Research Part II: Topical Studies in Oceanography* **49**(22-23): 5027-5047.
- 32 Matthews J. 1969. The assessment of a method for the determination of absolute pollen frequencies. *New*
33 *Phytologist* **68**(1): 161-166.
- 34 Matthiessen J. 1995. Distribution patterns of dinoflagellate cysts and other organic-walled microfossils in
35 recent Norwegian-Greenland Sea sediments. *Marine Micropaleontology* **24**: 307–334.
- 36 Matthiessen J, de Vernal A, Head M, *et al.* 2005. Modern organic-walled dinoflagellate cysts in arctic marine
37 environments and their (paleo-) environmental significance. *Paläontologische Zeitschrift* **79**(1): 3-51.
- 38 Mertens KN, Verhoeven K, Verleye T, *et al.* 2009. Determining the absolute abundance of dinoflagellate
39 cysts in recent marine sediments: the Lycopodium marker-grain method put to the test. *Review of*
40 *Palaeobotany and Palynology* **157**(3): 238-252.

- 1 Mertens KN, Van Nieuwenhove N, Gurdebeke PR, *et al.* 2018. The dinoflagellate cyst genera
2 *Achomosphaera* Evitt 1963 and *Spiniferites* Mantell 1850 in Pliocene to modern sediments: a summary
3 of round table discussions. *Palynology* **42**(sup1): 10-44.
- 4 Mudie PJ. 1992. Circum-Arctic Quaternary and Neogene marine palynofloras: paleoecology and statistical
5 analysis. *Neogene and Quaternary dinoflagellate cysts and acritarchs* **10**: 347-390.
- 6 Mudie PJ, Harland R, Matthiessen J, *et al.* 2001. Marine dinoflagellate cysts and high latitude Quaternary
7 paleoenvironmental reconstructions: an introduction. *Journal of Quaternary Science* **16**(7): 595-602.
- 8 Mudie PJ, Rochon A, Prins MA, *et al.* 2006. Late Pleistocene-Holocene Marine Geology of Nares Strait
9 Region: Palaeoceanography from Foraminifera and Dinoflagellate Cysts, Sedimentology and Stable
10 Isotopes. *Polarforschung* **74**(1-3): 169 – 183.
- 11 Münchow A, Melling H, Falkner KK. 2006. An observational estimate of volume and freshwater flux
12 leaving the Arctic Ocean through Nares Strait. *Journal of Physical Oceanography* **36**(11): 2025-2041.
- 13 Müller J, Stein R. 2014. High-resolution record of late glacial and deglacial sea ice changes in Fram Strait
14 corroborates ice-ocean interactions during abrupt climate shifts. *Earth and Planetary Science Letter* **403**:
15 446–455.
- 16 Ouellet-Bernier MM, de Vernal A, Hillaire-Marcel C, *et al.* 2014. Paleocceanographic changes in the Disko
17 Bugt area, West Greenland, during the Holocene. *The Holocene* **24**: 1573–1583.
- 18 Perner K, Moros M, Jennings AE, *et al.* 2013. Holocene palaeoceanographic evolution off West Greenland.
19 *The Holocene* **23**: 374–387.
- 20 Radi T, de Vernal A. 2008. Dinocysts as proxy of primary productivity in mid-high latitudes of the Northern
21 Hemisphere. *Marine Micropaleontology* **68**: 84–114.
- 22 Radi T, Bonnet S, Cormier MA, *et al.* 2013. Operational taxonomy and (paleo-) autecology of round, brown,
23 spiny dinoflagellate cysts from the Quaternary of high northern latitudes. *Marine Micropaleontology* **98**:
24 41-57.
- 25 Ribeiro S, Moros M, Ellegaard M, *et al.* 2012. Climate variability in West Greenland during the past 1500
26 years: Evidence from a high-resolution marine palynological record from Disko Bay. *Boreas* **41**: 68–83.
- 27 Rochon A, de Vernal A, Turon JL, *et al.* 1999. Distribution of recent dinoflagellate cysts in surface
28 sediments from the North Atlantic Ocean and adjacent seas in relation to sea-surface parameters.
29 *American Association of Stratigraphic Palynologists Contribution Series* **35**: 1-146.
- 30 Sadler HE. 1976. Water, heat, and salt transports through Nares Strait, Ellesmere Island. *Journal of the*
31 *Fisheries Research Board of Canada* **33**: 2286–2295.
- 32 Schweinsberg AD, Briner JP, Miller GH, *et al.* 2017. Local glaciation in West Greenland linked to North
33 Atlantic Ocean circulation during the Holocene. *Geology* **45**(3): 195-198.
- 34 Seidenkrantz MS, Roncaglia L, Fischel A, *et al.* 2008. Variable North Atlantic climate seesaw patterns
35 documented by a late Holocene marine record from Disko Bugt, West Greenland. *Marine*
36 *Micropaleontology* **68**: 66–83.
- 37 Serreze MC, Stroeve J. 2015. Arctic sea ice trends, variability and implications for seasonal ice forecasting.
38 *Philosophical Transactions of the Royal Society A* **373**(2045): 20140159.
- 39 Telford RJ. 2006. Limitations of dinoflagellate cyst transfer functions. *Quaternary Science Reviews* **25**(13-
40 14): 1375-1382.

- 1 Telford RJ, Birks HJB. 2005. The secret assumption of transfer functions: problems with spatial
2 autocorrelation in evaluating model performance. *Quaternary Science Reviews* **24**(20-21): 2173-2179.
- 3 Telford RJ, Birks HJB. 2011. A novel method for assessing the statistical significance of quantitative
4 reconstructions inferred from biotic assemblages. *Quaternary Science Reviews* **30**(9-10): 1272-1278.
- 5 Tang CCL, Ross CK, Yao T, *et al.* 2004. The circulation, water masses and sea-ice of Baffin Bay. *Progress*
6 *in Oceanography* **63**: 183–228.
- 7 Vinther BM, Buchardt SL, Clausen HB, *et al.* 2009. Holocene thinning of the Greenland ice sheet. *Nature*
8 **461**(7262): 385.
- 9 Zonneveld KAF, Marret F, Versteegh GJM, *et al.* 2013. Atlas of modern dinoflagellate cyst distribution
10 based on 2405 data points. *Review of Palaeobotany and Palynology* **191**: 1–197.
- 11 Zweng MM, Münchow A. 2006. Warming and freshening of Baffin Bay, 1916–2003. *Journal of*
12 *Geophysical Research: Oceans*, **111**(C07016).
- 13

1 **Table captions**

2

3 **Table 1.** Coordinates of the two cores used in this study.

Core ID	Region	Latitude (°N)	Longitude (°W)	Water depth (m)	Core length (cm)
AMD14-204	Upernavik Isstrøm	73°15.663'	57°53.987'	987	734
AMD14-Kane2B	Kane Basin	79°30.908'	70°49.742'	220	425

4

5

6 **Table 2.** List of the dominant dinoflagellate cyst taxa from the two cores location, shown in Fig.
7 2. G=Gonyaulacales, P=Peridinales, A=Autotrophic and H=Heterotrophic taxa.

Dinoflagellate taxa	Trophic mode		Grouped as
<i>Operculodinium centrocarpum</i> sensu Wall and Dale	G	A	<i>Operculodinium centrocarpum</i>
<i>O. centrocarpum</i> short processes	G	A	<i>Operculodinium centrocarpum</i>
<i>O. centrocarpum</i> Arctic	G	A	<i>Operculodinium centrocarpum</i>
<i>Nematosphaeropsis labyrinthus</i>	G	A	
<i>Spiniferites elongatus</i>	G	A	
<i>Spiniferites ramosus</i>	G	A	
Cyst of <i>Pentapharsodinium dalei</i>	P	A	
<i>Impagidinium pallidum</i>	G	A	
<i>Islandinium minutum</i>	P	H	
<i>Islandinium brevispinosum</i>	P	H	<i>Islandinium minutum</i>
<i>Islandinium? cezare</i>	P	H	<i>Islandinium minutum</i>
<i>Echinidinium karaense</i>	P	H	
<i>Brigantedinium</i> spp.	P	H	
<i>Brigantedinium simplex</i>	P	H	<i>Brigantedinium</i> spp.
<i>Brigantedinium cariacense</i>	P	H	<i>Brigantedinium</i> spp.
<i>Polykrikos</i> var. Arctic	P	H	
<i>Polykrikos quadratus</i>	P	H	<i>Polykrikos</i> var. Arctic

8

9

1 **Figures legends**

2
3 **Figure 1:** a) Map of Baffin Bay and Nares Strait indicating sampling location for cores AMD14-
4 Kane2B (Kane Basin) and AMD14-204 (Upernavik cross-shelf trough), as well as cores mentioned
5 in this study (MSM343300, sites 008 and 012, LS009). Regional surface oceanic circulation: BIC=
6 Baffin Island Current (Arctic water in blue); WGC = West Greenland Current (in red; mix of IC =
7 Irminger Current, North Atlantic water and EGC = East Greenland Current). NS: Nares Strait; MB:
8 Melville Bay; DB: Disko Bugt; DS: Davis Strait; LS: Lancaster Sound; SS: Smith Sound; NOW:
9 North Water Polynya. b) Satellite image of the study area indicating the sea ice cover (image from
10 22 May 2018; credit: NASA Worldview: <https://worldview.earthdata.nasa.gov>).

11
12 **Figure 2:** Photoplate of main dinocyst taxa and palynomorphs (foraminiferal lining) identified in
13 this study: a) *Operculodinium centrocarpum* sensu Wall and Dale; b) Cyst of *Pentapharsodinium*
14 *dalei*; c) *Nematosphaeropsis labyrinthus*; d) *Spiniferites elongatus*; e) *Spiniferites ramosus*; f)
15 *Impagidinium pallidum*; g) *Islandinium minutum*; h) *Echinidinium karaense*; i) *Polykrikos* var.
16 Arctic; j) *Brigantedinium simplex*; k) foraminiferal lining; l) *O centrocarpum* (left) + *I. minutum*
17 (right).

18
19 **Figure 3:** Dinocyst influx ($\times 10^2$ cysts $\text{cm}^{-2} \text{yr}^{-1}$), relative abundance (%) of the main dinocyst taxa,
20 and dinocyst assemblage zones in core AMD14-204. Data are represented with the thin dotted dark
21 grey lines, 3-points running mean are represented by green (autotrophs) or brown (heterotrophs)
22 lines.

23
24 **Figure 4:** Reconstructions of winter and summer salinity (SSS) and sea-surface temperature (SST),
25 seasonal sea-ice cover in months/year, and productivity (in $\text{gC m}^{-2} \text{yr}^{-1}$) based on the modern
26 analogue technique (MAT) applied to dinocyst assemblages in core AMD14-204. Reconstructions
27 are shown with the black lines, the 3-points running mean are represented by bold colored lines
28 and the maximum and minimum possible values according to the set of five analogues are shown
29 in light gray. Modern values are indicated by a black arrow at the top. Heterotrophs/Autotrophs
30 (H/A) ratio and influxes of organic linings of foraminifera, *Halodinium* sp. and reworked
31 palynomorphs are displayed on the right. Statistical minimum and maximum distances between
32 fossil and modern analogues are 0.12 and 0.20 respectively.

33
34 **Figure 5:** Dinocyst influx ($\times 10^2$ cysts $\text{cm}^{-2} \text{yr}^{-1}$), relative abundance (%) of the main dinocyst taxa,
35 and dinocyst assemblage zones in core AMD14-Kane2B. Data are represented with the thin dotted
36 dark grey lines, 3-points running mean are represented by green (autotrophs) or brown
37 (heterotrophs) lines. In samples containing sparse assemblages (counts < 50 cysts), occurrences are
38 reported by dots on the diagram.

39
40 **Figure 6:** Reconstructions of winter and summer salinity (SSS) and sea-surface temperature (SST),
41 seasonal sea-ice cover in months/year, and productivity (in $\text{gC m}^{-2} \text{yr}^{-1}$) based on modern analogue
42 technique (MAT) applied to dinocyst assemblages in core AMD14-Kane2B. Reconstructions are
43 shown with the black lines, the 3-points running means are represented by colored lines and the

1 maximum and minimum possible values according to the set of five analogues are shown in light
2 gray. Modern values are indicated by a black arrow at the top. Autotrophs/Heterotrophs (A/H)
3 ratio and influxes of organic linings of foraminifera, *Halodinium* sp. and reworked palynomorphs
4 are displayed on the right. Statistical minimum and maximum distances between fossil and modern
5 analogues are 0.08 and 0.11 respectively.

6
7 **Figure 7:** Comparison of the palynological records from core AMD14-204 (this study) with a) the
8 $\delta^{18}\text{O}$ of Camp Century (Vinther *et al.*, 2009), b-c: ‘North Atlantic’ taxa (*O. centrocarpum*, *S.*
9 *elongatus*, *S. ramosus*) relative abundance of (a) core MSM343300, Disko Bugt (Ouellet-Bernier
10 *et al.*, 2014) and (b) core 204, d-e: ‘Polar’ taxa (*I. minutum*, *E. karaense*, *Polykrikos* var. Arctic)
11 relative abundance (note reversed scale) of (d) core MSM343300 and (e) core 204, f) dinocysts
12 and foraminiferal linings influxes ($\text{cm}^{-2} \text{yr}^{-1}$) of core 204 and g) reconstructed SST anomaly ($^{\circ}\text{C}$)
13 compared to modern value for core 204. The Holocene Thermal Maximum is delimited by the two
14 dashed lines, and blue shaded areas indicate the two cold pulses (zones 2b and 2d).

15
16 **Figure 8:** Comparison of the palynological records from core AMD14-Kane2B (this study) with
17 a) the $\delta^{18}\text{O}$ temperature reconstructions from the Agassiz Ice Cap (Vinther *et al.*, 2009), b) SIC
18 duration (months/year) from sites 008 and 012 (Levac *et al.*, 2001), c) Gonyaulacal/Peridinoid
19 (G/P) ratio from site LS009 (Ledu *et al.*, 2008), d) ‘warm water’ taxa (*O. centrocarpum*, *S.*
20 *elongatus*) relative abundance from sites 008 and 012, e) foraminiferal lining influxes $\text{cm}^{-2} \text{yr}^{-1}$, f)
21 *O. centrocarpum* relative abundance, g) *I. minutum* relative abundance, h) dinocyst influxes in cyst
22 $\text{cm}^{-2} \text{yr}^{-1}$. Data from sites 008, 012 and LS009 (core 2004-804-009) were downloaded from the
23 GEOTOP dinocyst database (de Vernal *et al.*, 2013a).

25 **Supplementary material**

26 Additional supporting information:

27 **Fig. S1.** High-resolution images, CT-Scan, age models and sedimentary units for cores AMD14-
28 204 and AMD14-Kane2B. Radiocarbon dates are from Georgiadis *et al.* (2018) for Kane2B and
29 from Caron *et al.* (2019) for core 204; paleomagnetic stratigraphic markers from Caron *et al.* (2019)
30 and organic matter is from Giraudeau *et al.* (under revision). RDL: Rapidly deposited layer.

31
32 **Fig. S2.** Results of the principal component analysis as a function of depth (cm) for cores AMD14-
33 204 and AMD14-Kane2B. PC scores are given at the top of each graph, which represent >95%
34 total variance. Dark grey shade (300-320 cm) in core Kane2B corresponds to the RDL (Rapidly
35 Deposited Layer) which marks the final opening of Nares Strait (Georgiadis *et al.*, 2018).

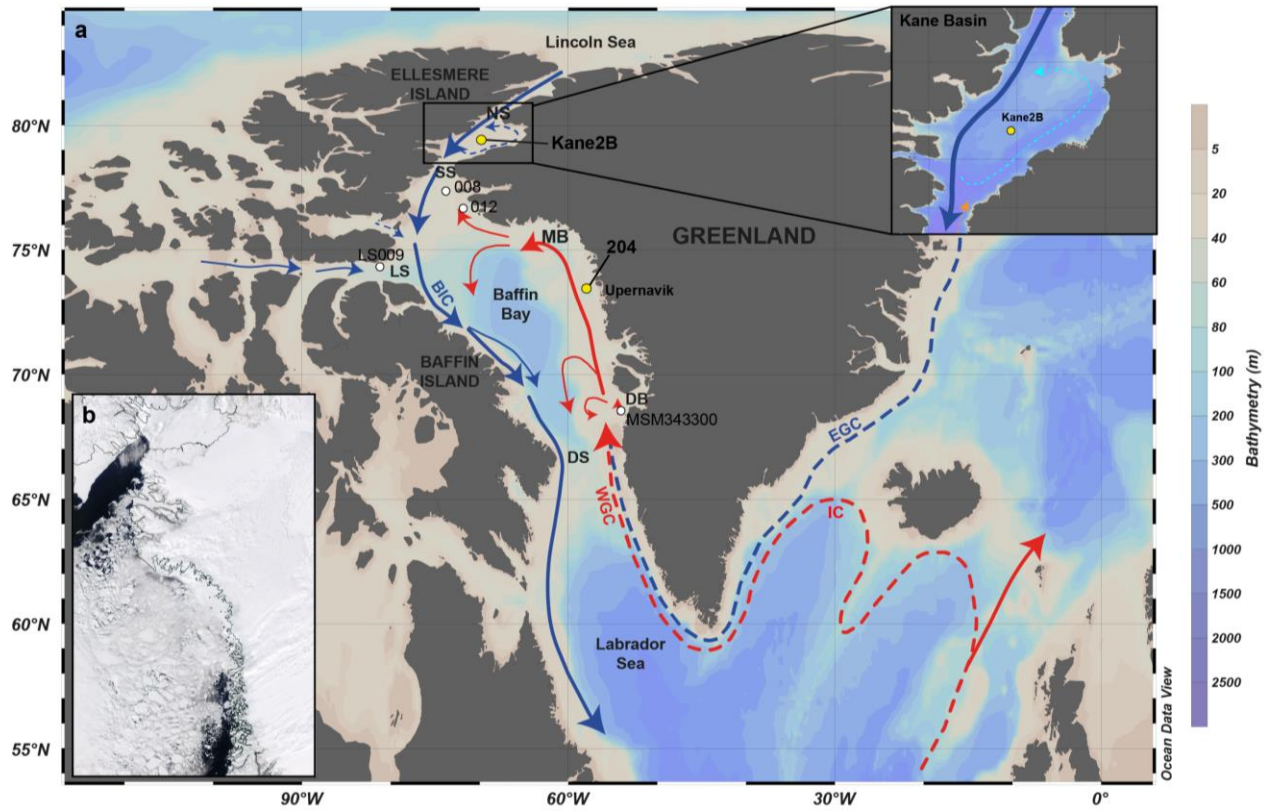


Figure 1

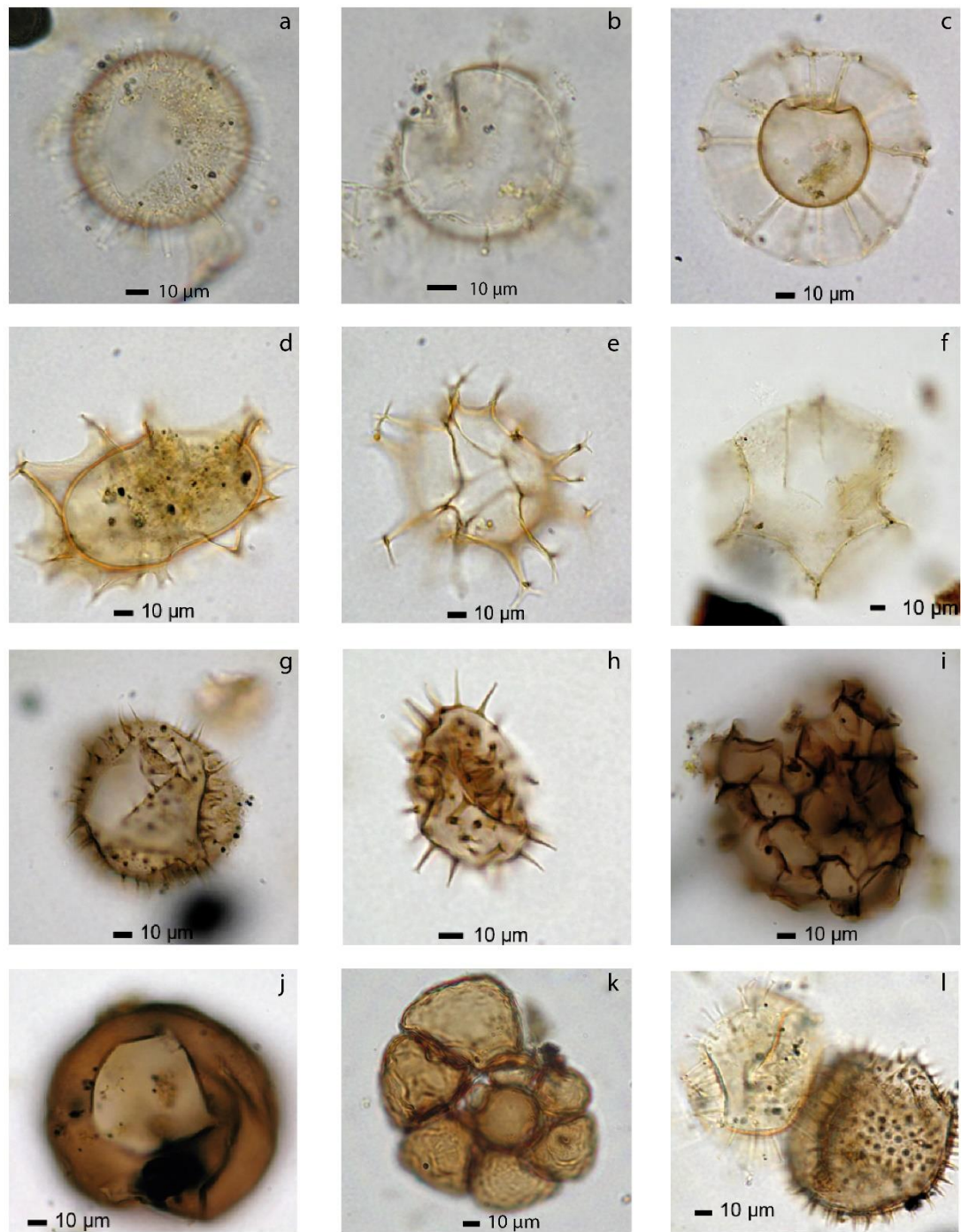


Figure 2

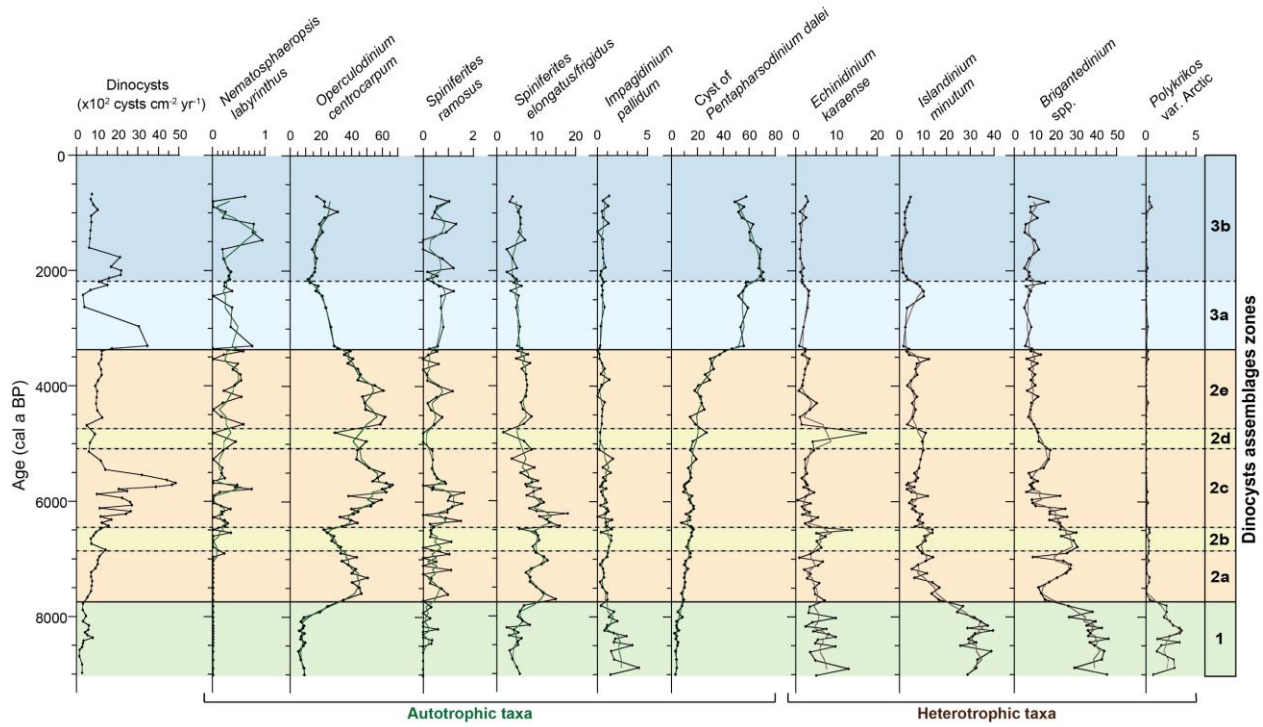


Figure 3

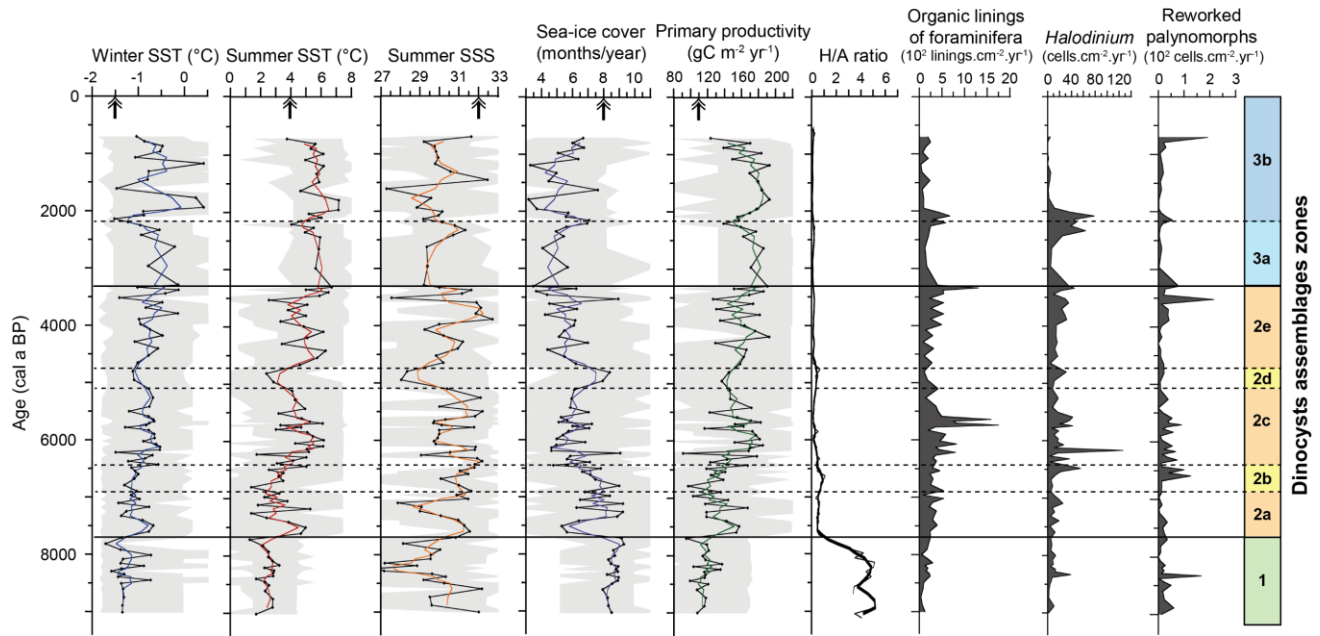


Figure 4

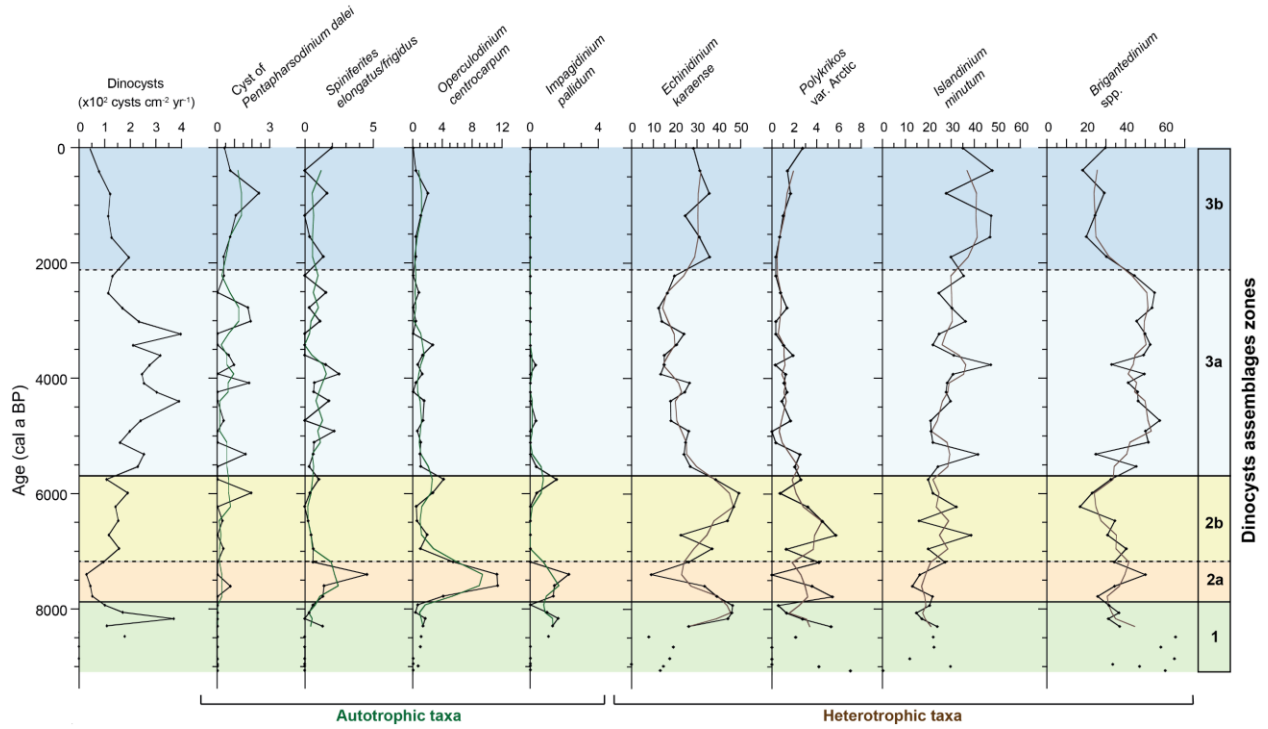


Figure 5

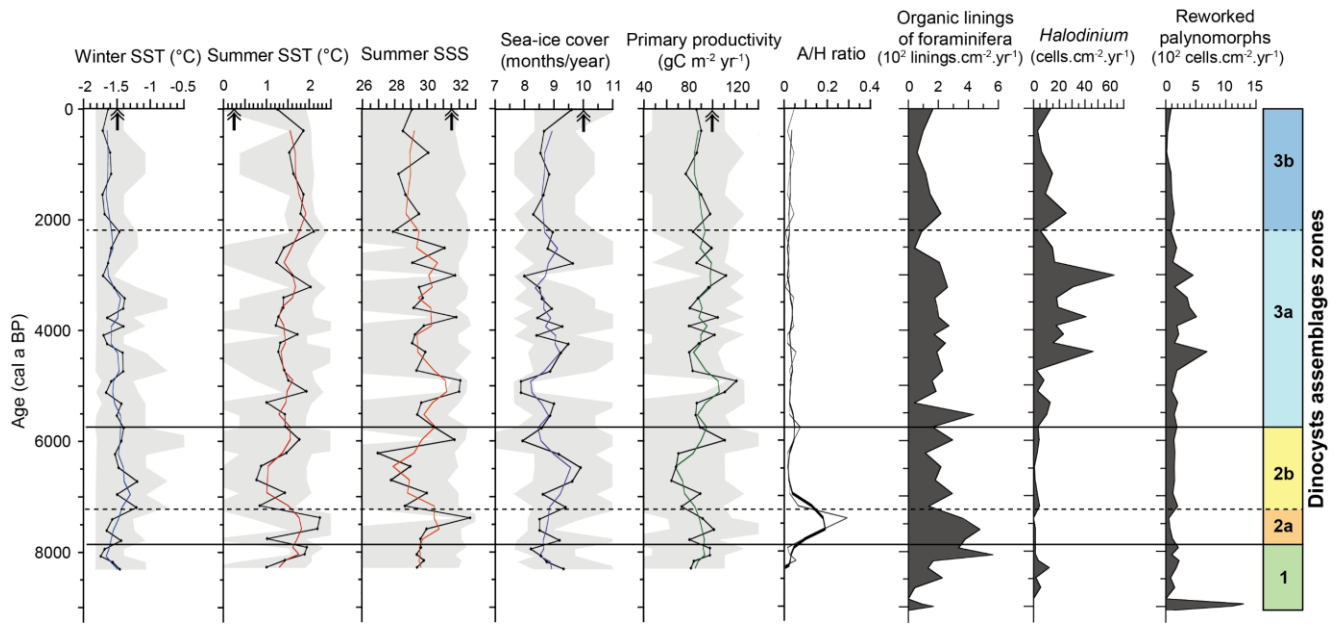


Figure 6

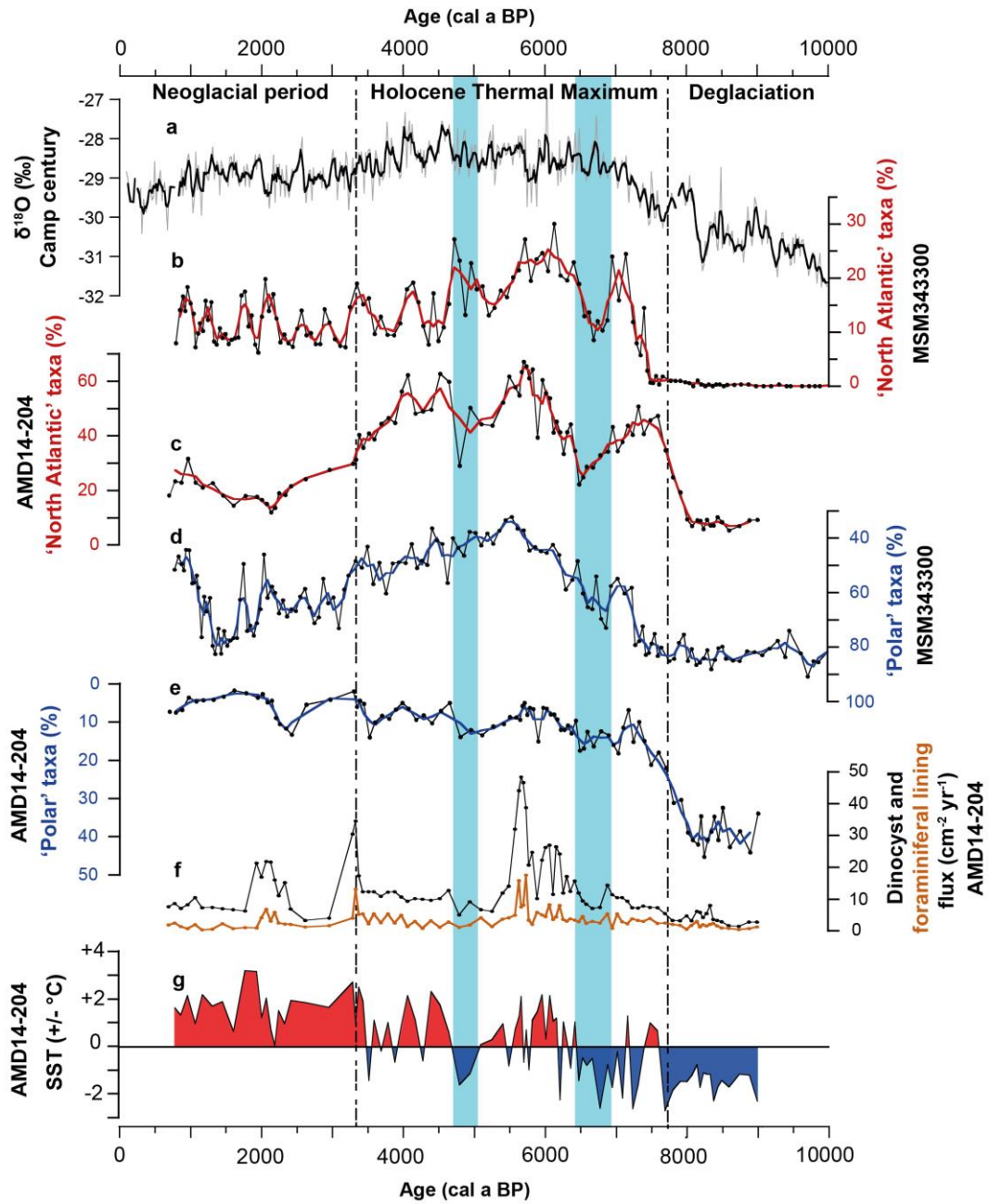


Figure 7

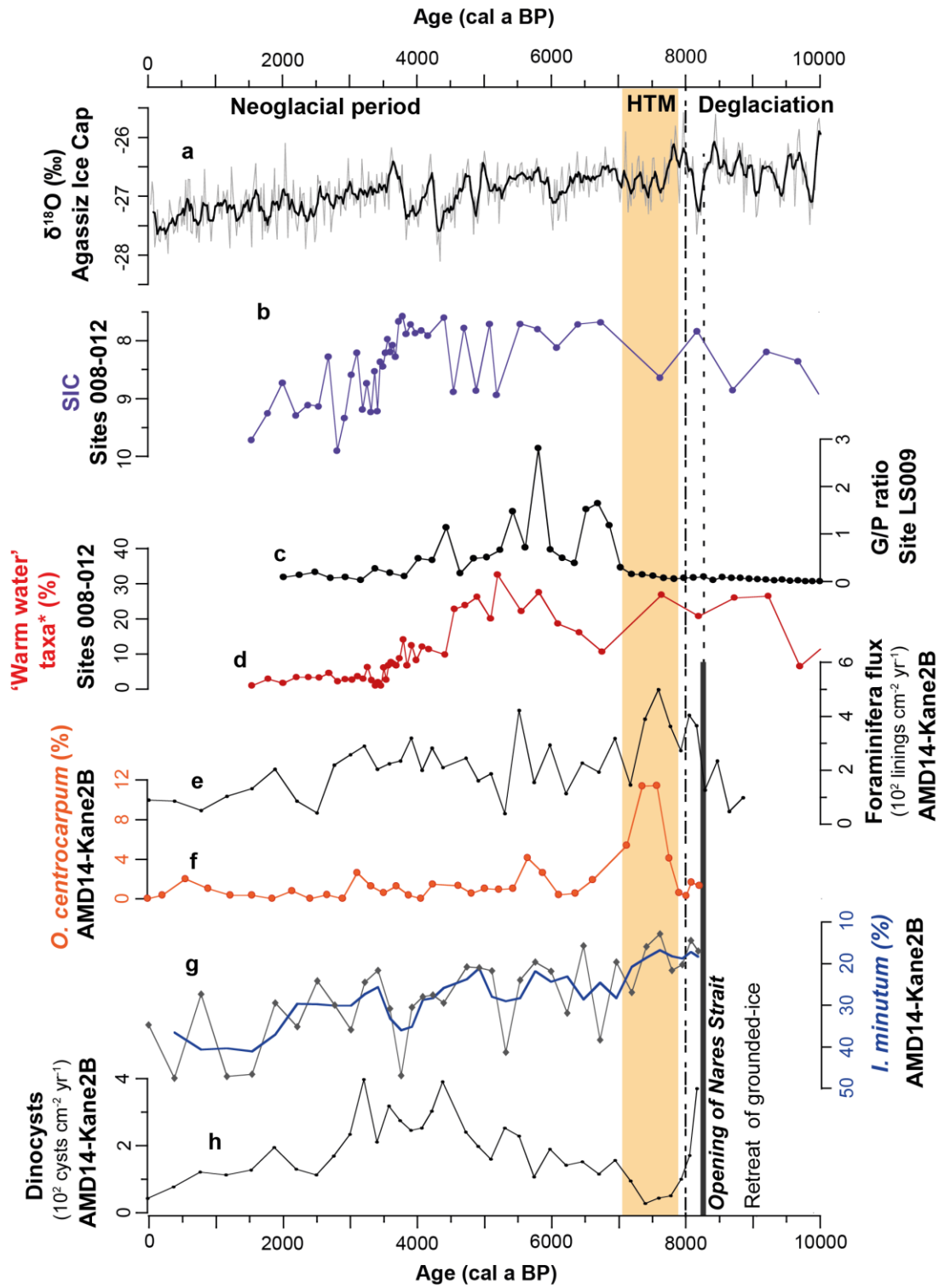


Figure 8

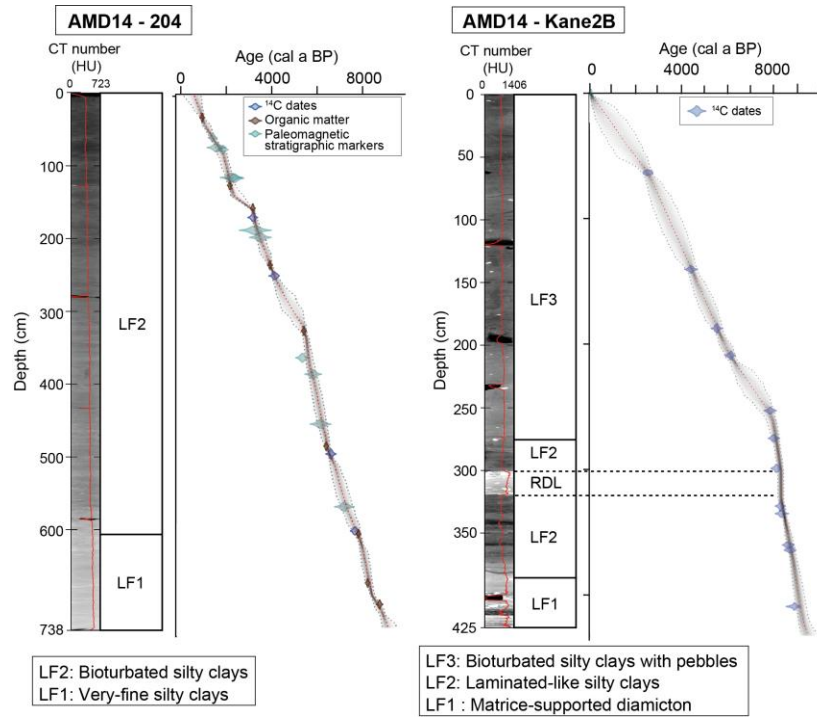


Figure S1

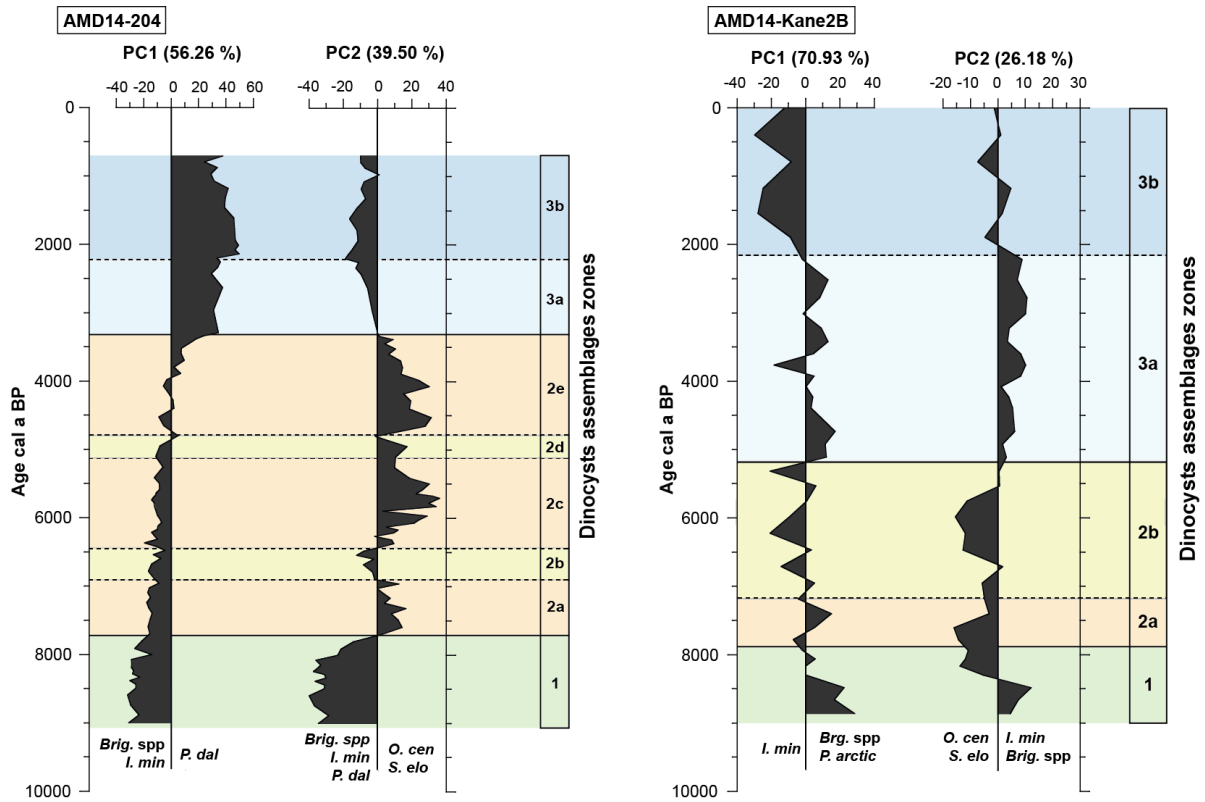


Figure S2